Quantum Simulation of Topological Zero Modes on a 41-Qubit Superconducting Processor

Yun-Hao Shi [1,2,3,*] Yu Liu [1,2,*] Yu-Ran Zhang [4,5,6,*] Zhongcheng Xiang [1,2,*] Kaixuan Huang,[3] Tao Liu,[4]
Yong-Yi Wang,[1,2] Jia-Chi Zhang,[1,2] Cheng-Lin Deng,[1,2] Gui-Han Liang,[1,2] Zheng-Yang Mei,[1,2] Hao Li,[1] Tian-Ming Li,[1,2]
Wei-Guo Ma,[1,2] Hao-Tian Liu,[1,2] Chi-Tong Chen,[1,2] Tong Liu [1,2] Ye Tian,[1] Xiaohui Song,[1] S. P. Zhao,[1,2,7]
Kai Xu [1,2,3,7,8,†] Dongning Zheng [1,2,7,8,‡] Franco Nori,[5,6,9,§] and Heng Fan [1,2,3,7,8,10,‖]

[1]*Institute of Physics, Chinese Academy of Sciences, Beijing 100190, China*
[2]*School of Physical Sciences, University of Chinese Academy of Sciences, Beijing 100049, China*
[3]*Beijing Academy of Quantum Information Sciences, Beijing 100193, China*
[4]*School of Physics and Optoelectronics, South China University of Technology, Guangzhou 510640, China*
[5]*Theoretical Quantum Physics Laboratory, Cluster for Pioneering Research, RIKEN, Wako-shi, Saitama 351-0198, Japan*
[6]*Center for Quantum Computing, RIKEN, Wako-shi, Saitama 351-0198, Japan*
[7]*Songshan Lake Materials Laboratory, Dongguan, Guangdong 523808, China*
[8]*CAS Center for Excellence in Topological Quantum Computation, UCAS, Beijing 100049, China*
[9]*Physics Department, University of Michigan, Ann Arbor, Michigan 48109-1040, USA*
[10]*Hefei National Laboratory, Hefei 230088, China*

Quantum simulation of different exotic topological phases of quantum matter on a noisy intermediate-scale quantum (NISQ) processor is attracting growing interest. Here, we develop a one-dimensional 43-qubit superconducting quantum processor, named *Chuang-tzu*, to simulate and characterize emergent topological states. By engineering diagonal Aubry-André-Harper (AAH) models, we experimentally demonstrate the Hofstadter butterfly energy spectrum. Using Floquet engineering, we verify the existence of the topological zero modes in the commensurate off-diagonal AAH models, which have never been experimentally realized before. Remarkably, the qubit number over 40 in our quantum processor is large enough to capture the substantial topological features of a quantum system from its complex band structure, including Dirac points, the energy gap's closing, the difference between even and odd number of sites, and the distinction between edge and bulk states. Our results establish a versatile hybrid quantum simulation approach to exploring quantum topological systems in the NISQ era.

The Aubry-André-Harper (AAH) model [1,2] has been attracting considerable attention in various topics of condensed matter physics, including Hofstadter butterfly [3,4], Anderson localization [5], quasicrystals [6], and topological phases of matter [7,8]. The incommensurate diagonal AAH model describes a one-dimensional (1D) tight bonding lattice with quasiperiodic potential. In this model a localization transition is predicted [2], which has been observed experimentally [9,10]. Moreover, the diagonal AAH model can be exactly mapped to the two-dimensional (2D) Hofstadter model [3], showing a 2D quantum Hall effect (QHE) with topologically protected edge states, which have been observed in experiments [6,11]. The energy spectra of Bloch electrons in perpendicular magnetic fields versus the dimensional perpendicular magnetic field b form the Hofstadter butterfly [3,4], showing the splitting of energy bands for a specific value of b. The Hofstadter butterfly energy spectrum has been measured in quasiperiodic lattices [12–14], superlattices [15–17], and Floquet dissipative quasicrystal [18]. A further generalization to commensurate off-diagonal AAH models, with the hopping amplitude being cosine-modulated commensurate with the lattice, indicates the existence of topological zero-energy edge states in the gapless regime [19]. The topological zero modes differ from the edge states in the 1D diagonal AAH models (similar to the quantum Hall edge) and have never been observed in experiments before.

Rapid developments in quantum techniques allow for programming nontrivial topological models and observing their topological states on quantum simulating platforms with a fast-growing number of qubits [11,20–22]. Even without fault tolerance, the programmability of a noisy intermediate-scale quantum (NISQ) processor helps to explore various topological phases that are still challenging in real materials [23–27]. Here, we develop a 43-qubit superconducting quantum processor arranged in a 1D array, named *Chuang-tzu* [Fig. 1(a)], to simulate the generalized 1D AAH model. The mean energy relaxation time and pure dephasing time of 41 qubits in our experiments are 21.0 and 1.2 μs, respectively. Since our processor is designed to
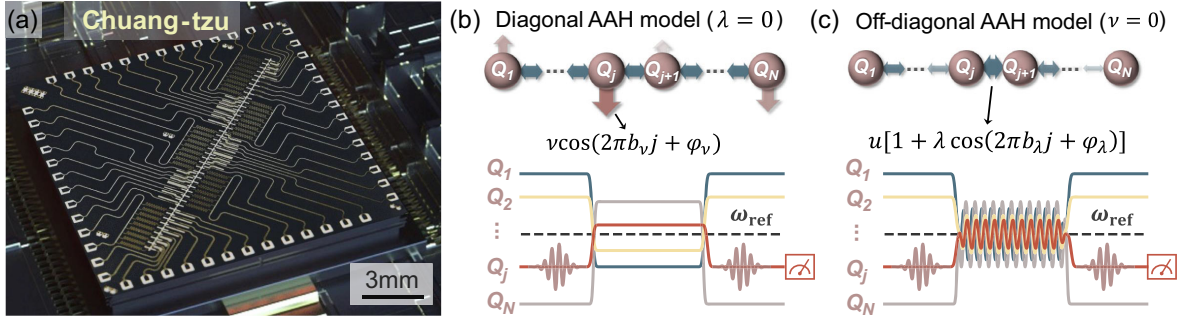
FIG. 1.   Device and pulse sequences. (a) Optical micrograph of the 43-qubit quantum chip. (b) Diagonal AAH model simulated by periodically tuning the qubit's frequency and the pulse sequence for its band structure spectroscopy. (c) Off-diagonal AAH model engineered by Floquet engineering qubit's frequency and the pulse sequence for its band structure spectroscopy.

fulfill the hard-core limit [11,28], the effective Hamiltonian reads

$$\hat{H}_0 = \sum_{j=1}^{N-1} g_{j,j+1}(\hat{a}_j^\dagger \hat{a}_{j+1} + \text{H.c.}) + \sum_{j=1}^{N} \omega_j \hat{a}_j^\dagger \hat{a}_j, \quad (1)$$

where $\hat{a}^\dagger$ ($\hat{a}$) denotes the hard-core bosonic creation (annihilation) operator. In our sample, the frequency ω_j of each qubit Q_j is tunable, but the hopping strength $g_{j,j+1}$ between nearest-neighbor (NN) Q_j and Q_{j+1} cannot be tuned directly. Here we use the Floquet engineering technique as demonstrated in [29–35] to simulate the generalized 1D AAH model with a form

$$\hat{H}_{\text{gAAH}} = \sum_{j=1}^{N-1} u[1 + \lambda \cos(2\pi b_\lambda j + \varphi_\lambda)](\hat{a}_j^\dagger \hat{a}_{j+1} + \text{H.c.})$$
$$+ \sum_{j=1}^{N} v \cos(2\pi b_v j + \varphi_v)\hat{a}_j^\dagger \hat{a}_j, \quad (2)$$

with $\lambda = 0$ and $v = 0$ corresponding to the diagonal and off-diagonal AAH models, respectively. In our system, we can independently vary the effective on-site potential ω_j^{eff} and the effective hopping strength $g_{j,j+1}^{\text{eff}}$ by the rectangle flux bias and time-periodic driving on the Z control lines of qubits, respectively. The effective $g_{j,j+1}^{\text{eff}}$ can be adjusted from about -3.0 to 7.6 MHz. Thus, the dynamics of the generalized AAH models are simulated with an approximately effective Hamiltonian using Floquet engineering, and our simulator behaves as a programmable hybrid analog-digital quantum simulator from the viewpoint in [25]. Details of tuning hopping strength via Floquet engineering are discussed in [36].

First, we engineer the diagonal AAH model [40,41] with $N = 41$ qubits and measure the Hofstadter butterfly spectrum in the quasiperiodic lattices by setting $\lambda = 0$ and tuning the on-site potential as $v \cos(2\pi b_v j)$ with $v/(2\pi) \simeq 15.2$ MHz and $\varphi_v = 0$ [Fig. 1(b)]. We simulate 121

instances of diagonal AAH chains when varying b_v from 0 to 1. Using the band structure spectroscopic technique [11,12], we obtain the squared Fourier transformation (FT) magnitude $|\tilde{\chi}_j|^2$ of the response function $\chi_j(t) \equiv \langle \hat{\sigma}_j^x(t) \rangle + i\langle \hat{\sigma}_j^y(t) \rangle$, after preparing a selected qubit Q_j at $|+\rangle_j = (|0_j\rangle + |1_j\rangle)/\sqrt{2}$. Figure 2(a) plots $|\tilde{\chi}_j|^2$ for several selected qubits Q_j, and each of them only contains partial information about the energy spectrum. The summation of the squared FT magnitudes [Fig. 2(b)] of all chosen qubits $I_{b_v} \equiv \sum_j |\tilde{\chi}_j|^2$ clearly shows the Hofstadter butterfly energy spectrum, which agrees well with the numerical calculation by simulating the system's dynamics [Fig. 2(c)] and the theoretical prediction [Fig. 2(d)]. Note that the fractal structure of "Hofstadter's butterfly," splitting of energy bands for several b_v, are clearly shown, which is attributed to the sufficiently large qubit number of our quantum processor [13]. In addition, the winglike gaps emerge because of the topological feature of the diagonal AAH models, and the 2D integer QHE is characterized by the Chern number [42], which has been experimentally investigated in [11] for $b_v = 1/3$.

Next, we perform a hybrid analog-digital quantum simulation of the off-diagonal AAH models with $v = 0$ and $\lambda \neq 0$ using Floquet engineering [30] [Fig. 1(c)], which show no QHE [19]. With the bulk-edge correspondence [11,43], we characterize their topological zero-energy modes, of which the experimental observation is still absent. We first engineer the commensurate off-diagonal AAHs for $b_\lambda = 1/2$ that can be mapped to a 2D Hofstadter model with π flux per plaquette. We experimentally extract the band structures of the lattices with $N = 40$ (even) and 41 (odd) sites by measuring I_{φ_λ} for $\varphi_\lambda \in [0, 2\pi]$ as shown in Figs. 3(a) and 3(b), respectively, which agrees well with the theoretical prediction (dashed curves). The measured gapless band structure clearly shows two Dirac points with a linear dispersion, which is similar to those observed in graphene [19]. On the lattice with $N = 40$ (even) sites, two topological zero modes appear for $\varphi_\lambda \in (-\pi/2, \pi/2)$ [Fig. 3(a)], while the topological zero edge mode exists
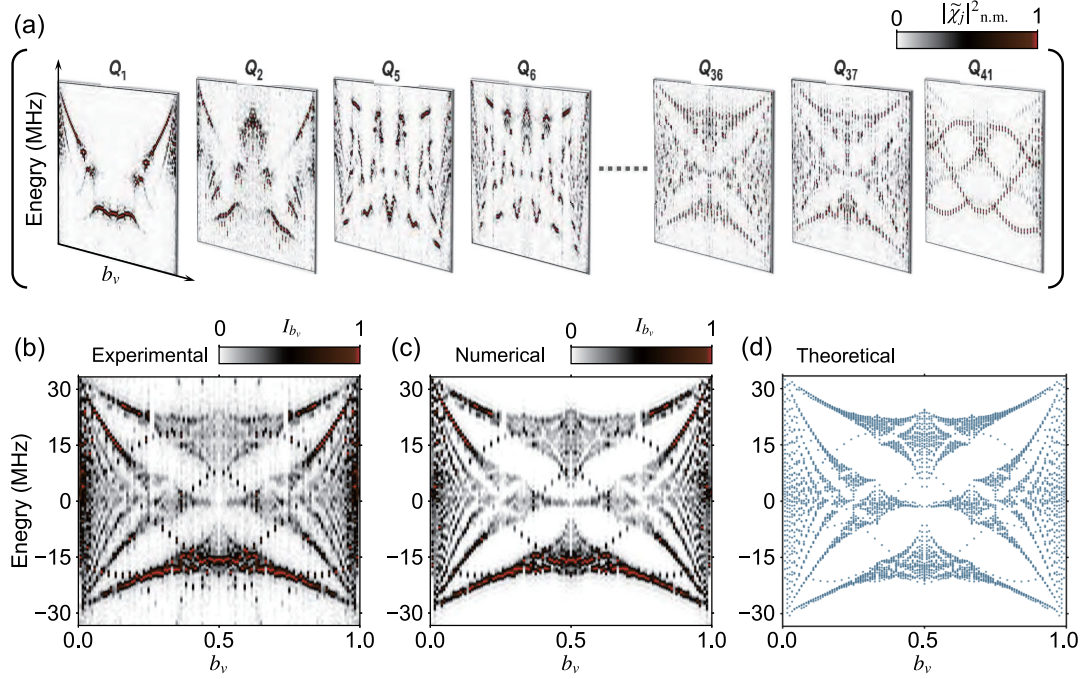
FIG. 2. Hofstadter butterfly energy spectrum. By engineering various instances of AAH models, the energy spectrum of the Bloch electrons in perpendicular magnetic fields can be measured using band structure spectroscopy [11,12]. Here we use $N = 41$ qubits to simulate the quasiperiodic lattice. (a) Experimentally measured squared FT magnitudes $|\tilde{\chi}_j|^2$ when choosing a target qubit Q_j. (b)–(d) Experimental data of $I_{b_v} \equiv \sum_j |\tilde{\chi}_j|^2$ (b), the summation of the squared FT magnitudes, which is compared with the numerical data by simulating the dynamics of the system (c), and the theoretical prediction (d).

for the whole parameter regime [Fig. 3(b)] with $N = 41$ (odd) sites. These exotic topological edge states are also verified from the experimentally measured squared FT magnitudes $|\tilde{\chi}_j|^2$ for boundary qubits, as shown in Figs. 3(c)–3(f). For even sites, the $|\tilde{\chi}_1|^2$ [Fig. 3(c)] and $|\tilde{\chi}_{40}|^2$ [Fig. 3(d)] for Q_1 and Q_{40}, respectively, both contain information of topological zero edge states in the regime $(-\pi/2, \pi/2)$. However, for odd sites, the $|\tilde{\chi}_1|^2$ [Fig. 3(e)] for Q_1 shows left edge state for $(-\pi/2, \pi/2)$ and the Q_{41}'s $|\tilde{\chi}_{41}|^2$ [Fig. 3(f)] implies the existence of the right edge mode for $(\pi/2, 3\pi/2)$. The small shift of the zero energy of the edge state is attributed to the existence of weak next-nearest-neighboring (NNN) hopping (with an average of about 0.7 MHz) of our sample that slightly breaks the particle-hole symmetry; see details in [36]. Our experiments therefore verify the robustness of the topological zero-energy edge states in the commensurate off-diagonal AAH models.

Furthermore, the topological edge state can also be identified in real space by witnessing the localization of an edge excitation during its quantum walks (QWs) on the 1D qubit chain [11,29], due to its main overlap with the edge state. We monitor the time evolution of the excitation probabilities P_j for all qubits during the QWs. For even sites, QWs of an excitation at either boundary qubit present localization for $\varphi_\lambda = 0$ [Figs. 3(g) and 3(h)] in the topological regime and dispersion for $\varphi_\lambda = \pi$ [Figs. 3(i)

and 3(j)] in the trivial regime, respectively. In comparison, as shown in Figs. 3(k)–3(n), the QWs of an excitation at Q_1 (Q_{41}) shows localization (diffusion) for $\varphi_\lambda = 0$ and diffusion (localization) for $\varphi_\lambda = \pi$. Thus, our experimental results assert that there always exists only one zero-energy mode localized at either edge in the commensurate off-diagonal AAH models for π flux with odd sites. Note that it is still challenging to observe these different behaviors of topological edge modes between even and odd sites in real materials or some other quantum simulating platforms without a fixed number of lattice sites. In our NISQ device, the individually addressable superconducting qubits assisted by Floquet engineering help to overcome these difficulties and show its potential for investigating various exotic topological phenomena.

As the π-flux off-diagonal AAH model can be mapped to the Su-Schrieffer-Heeger (SSH) model [44], the off-diagonal AAH models as a new class of topological models are given by $b_\lambda = 1/(2q)$ with an integer $q > 1$ [19]. Here, we apply 40 qubits to experimentally investigate the generic off-diagonal AAH model for $b_\lambda = 1/4$ by tuning $g_{j,j+1}^{\text{eff}} = u[1 + \lambda \cos(2\pi b_\lambda j + \varphi_\lambda)]$, with φ_λ varying from 0 to 2π. This model has four energy bands, and the top and bottom bands are fully gapped, where the quantum Hall edge states are clearly exhibited from the measured band structure, see Fig. 4. By tuning $\lambda = \sqrt{2}$, we see that the central gap closes as theoretically predicted in [19], see
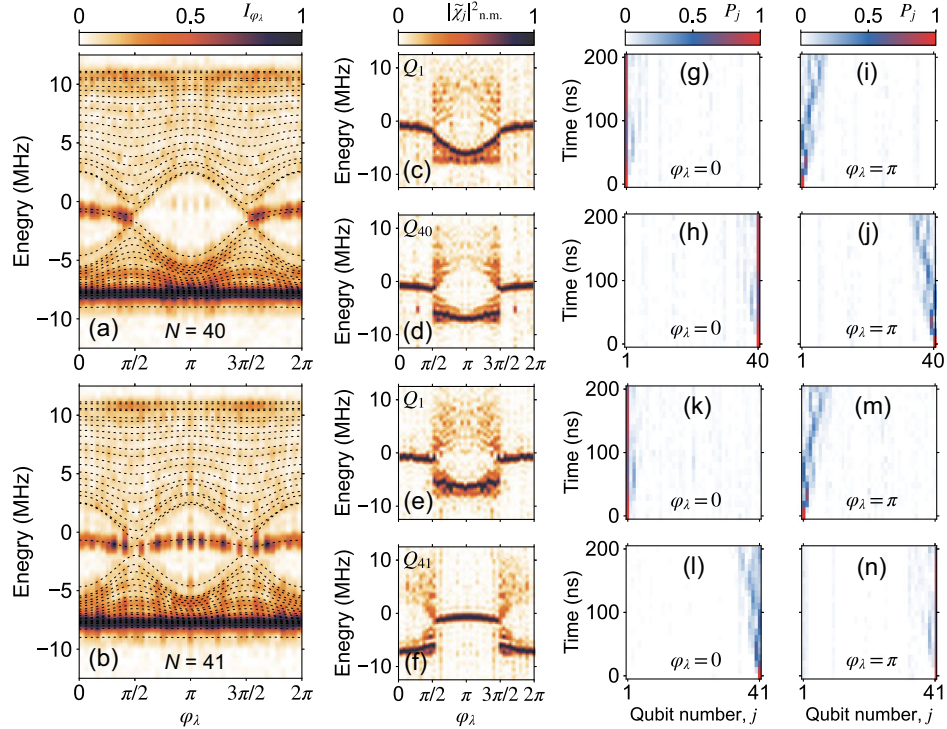
FIG. 3. Experimental characterization of the topological zero-energy edge modes in commensurate off-diagonal AAH models for π flux ($b_\lambda = 1/2$). Band structure spectroscopy of off-diagonal AAH models with even number $N = 40$ (a) and odd number $N = 41$ (b) of sites, which are compared with the theoretical projected band structures (dashed curves). Here $u/(2\pi) = 4.78$ MHz and $\lambda = 0.4$. Normalized squared FT magnitudes $|\tilde{\chi}_j|^2_{\text{n.m.}}$ when choosing the leftmost qubit Q_1 (c) and the rightmost qubit Q_{40} (d) as target qubits with $N = 40$. $|\tilde{\chi}_j|^2_{\text{n.m.}}$ for boundary qubits Q_1 (e) and Q_{41} (f) as target qubits with $N = 41$. (g)–(j) Time evolution of the excitation probability P_j during the QWs of a single excitation initially prepared at the boundary qubits (Q_1 or Q_{40}) for $\varphi_\lambda = 0$ (g),(h) and $\varphi_\lambda = \pi$ (i),(j) with $N = 40$. (k)–(n) Time evolution of P_j during the QWs of a single excitation initially placed at the boundary qubits (Q_1 or Q_{41}) for $\varphi_\lambda = 0$ (k),(l) and $\varphi_\lambda = \pi$ (m),(n) with $N = 41$.

Fig. 4(a), which is difficult to be realized with a small-scale quantum simulator. Then, we tune $\lambda = 1$ and measure the band structure as shown in Fig. 4(b), where the central two bands are shown to have four band crossing points near $\varphi_\lambda = \pi/4$, $3\pi/4$, $5\pi/4$, and $7\pi/4$. Although the midgap is very small to observe, we can imply from the measured energy spectrum [Fig. 4(b)] that the central two bands are gapped in the regime $(-\pi/4, \pi/4)$ and $(3\pi/4, 5\pi/4)$; the
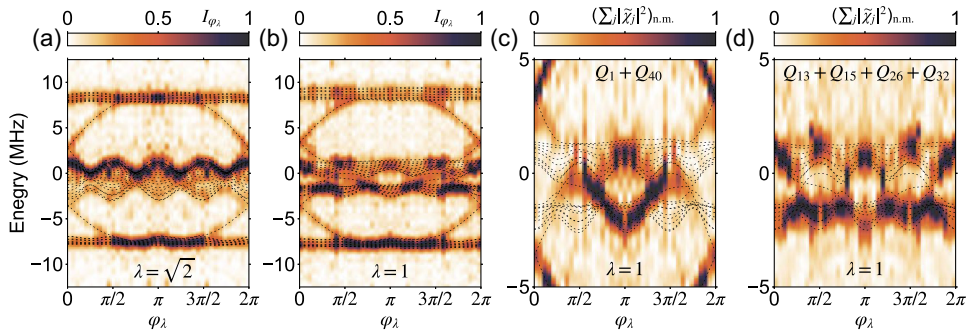
FIG. 4. Band structure spectroscopy of generic commensurate off-diagonal AAH models with $N = 40$ for $b_\lambda = 1/4$. (a) Experimental I_{φ_λ} for $\lambda = \sqrt{2}$ and $u/(2\pi) = 2.77$ MHz. The gap between two central bands closes, and no topological edge states between these two bands are observed. (b) Experimental I_{φ_λ} for $\lambda = 1$ and $u/(2\pi) = 3.35$ MHz. The two central bands are clearly observed gapped without edge modes in the regimes $\varphi_\lambda \in (-\pi/4, \pi/4)$ and $(3\pi/4, 5\pi/4)$. (c) Normalized FT magnitudes of two boundary qubits $(|\tilde{\chi}_1|^2 + |\tilde{\chi}_{40}|^2)_{\text{n.m.}}$, compared with the theoretical projected band structures (dashed curves). The topologically nontrivial zero-energy modes are observed between two central bands. (d) Four bulk qubits $(\sum_{j=13,15,26,32} |\tilde{\chi}_j|^2)_{\text{n.m.}}$, compared to the theoretical projected band structures (dashed curves). Four band crossing points are observed near $\varphi_\lambda = \pi/4$, $3\pi/4$, $5\pi/4$, and $7\pi/4$.

topological edge states appear in the regime $(\pi/4, 3\pi/4)$ and $(5\pi/4, 7\pi/4)$. To further analyze these two central bands, we separately study the edge and bulk states from the FT signals by only considering the boundary and bulk qubits, respectively. In Fig. 4(c), we plot the summation of the squared FT magnitudes of two boundary qubits Q_1 and Q_{40} versus φ_λ, which mainly shows the information for both the quantum Hall edges in the top and bottom gaps and the zero-energy edges between two central bands. We also illustrate in Fig. 4(d) the summed FT signals for selected bulk qubits Q_{13}, Q_{15}, Q_{26}, and Q_{32}, indicating the existence of four band crossing points. Note that the NNN hopping merely causes the shift of zero-energy edge states to mid-gap edges, which verifies the robustness of the topological properties of the commensurate off-diagonal AAH model.

In summary, we experimentally measure the celebrated Hofstadter butterfly energy spectra of up to 41 superconducting qubits and verify the existence of topological zero-energy edge modes in the gapless commensurate AAH models. We introduce multi-qubit Floquet engineering in superconducting circuits, which can be used to realize a wider range of models in condensed matter physics than AAH models, e.g., lattice gauge theories [45] and non-Hermitian systems [46]. In addition, we provide a general automatic calibration scheme for the devices with Floquet engineering (see details in [36]), which is also adaptable to other quantum simulating platforms. Our universal 1D hybrid analog-digital quantum simulator shows the potential to use programmable NISQ device to investigate exotic topological phases of quantum matter that is still arduous to do in real materials.

---

*These authors contributed equally to this work.

†kaixu@iphy.ac.cn

‡dzheng@iphy.ac.cn

§fnori@riken.jp

‖hfan@iphy.ac.cn

[1] P. G. Harper, Single band motion of conduction electrons in a uniform magnetic field, Proc. Phys. Soc. London Sect. A **68**, 874 (1955).

[2] S. Aubry and G. André, Analyticity breaking and Anderson localization in incommensurate lattices, Ann. Isr. Phys. Soc. **3**, 18 (1980).

[3] D. R. Hofstadter, Energy levels and wave functions of Bloch electrons in rational and irrational magnetic fields, Phys. Rev. B **14**, 2239 (1976).

[4] Y. Hatsugai and M. Kohmoto, Energy spectrum and the quantum Hall effect on the square lattice with next-nearest-neighbor hopping, Phys. Rev. B **42**, 8282 (1990).

[5] P. W. Anderson, Absence of diffusion in certain random lattices, Phys. Rev. **109**, 1492 (1958).

[6] Y. E. Kraus, Y. Lahini, Z. Ringel, M. Verbin, and O. Zilberberg, Topological States and Adiabatic Pumping in Quasicrystals, Phys. Rev. Lett. **109**, 106402 (2012).

[7] M. Z. Hasan and C. L. Kane, Colloquium: Topological insulators, Rev. Mod. Phys. **82**, 3045 (2010).

[8] X.-L. Qi and S.-C. Zhang, Topological insulators and superconductors, Rev. Mod. Phys. **83**, 1057 (2011).

[9] Y. Lahini, R. Pugatch, F. Pozzi, M. Sorel, R. Morandotti, N. Davidson, and Y. Silberberg, Observation of a Localization Transition in Quasiperiodic Photonic Lattices, Phys. Rev. Lett. **103**, 013901 (2009).

[10] H. Li, Y.-Y. Wang, Y.-H. Shi, K. Huang, X. Song, G.-H. Liang, Z.-Y. Mei, B. Zhou, H. Zhang, J.-C. Zhang, S. Chen, S. P. Zhao, Y. Tian, Z.-Y. Yang, Z. Xiang, K. Xu, D. Zheng, and H. Fan, Observation of critical phase transition in a generalized Aubry-André-Harper model with superconducting circuits, npj Quantum Inf. **9**, 40 (2023).

[11] Z.-C. Xiang, K. Huang, Y.-R. Zhang, T. Liu, Y.-H. Shi, C.-L. Deng, T. Liu, H. Li, G.-H. Liang, Z.-Y. Mei, H. Yu, G. Xue, Y. Tian, X. Song, Z.-B. Liu, K. Xu, D. Zheng, F. Nori, and H. Fan, Simulating Chern insulators on a superconducting quantum processor, arXiv:2207.11797.

[12] P. Roushan et al., Spectroscopic signatures of localization with interacting photons in superconducting qubits, Science **358**, 1175 (2017).

[13] X. Ni, K. Chen, M. Weiner, D. J. Apigo, C. Prodan, A. Alù, E. Prodan, and A. B. Khanikaev, Observation of Hofstadter butterfly and topological edge states in reconfigurable quasiperiodic acoustic crystals, Commun. Phys. **2**, 55 (2019).

[14] D. Hangleiter, I. Roth, J. Eisert, and P. Roushan, Precise Hamiltonian identification of a superconducting quantum processor, arXiv:2108.08319.

[15] C. R. Dean, L. Wang, P. Maher, C. Forsythe, F. Ghahari, Y. Gao, J. Katoch, M. Ishigami, P. Moon, M. Koshino, T. Taniguchi, K. Watanabe, K. L. Shepard, J. Hone, and P. Kim, Hofstadter's butterfly and the fractal quantum Hall effect in moiré superlattices, Nature (London) **497**, 598 (2013).

[16] X. Lu, B. Lian, G. Chaudhary, B. A. Piot, G. Romagnoli, K. Watanabe, T. Taniguchi, M. Poggio, A. H. MacDonald, B. A. Bernevig, and D. K. Efetov, Multiple flat bands and topological Hofstadter butterfly in twisted bilayer graphene close to the second magic angle, Proc. Natl. Acad. Sci. U.S.A. **118**, e2100006118 (2021).

[17] A. V. Rozhkov, A. O. Sboychakov, A. L. Rakhmanov, and F. Nori, Electronic properties of graphene-based bilayer systems, Phys. Rep. **648,** 1 (2016).

[18] S. Weidemann, M. Kremer, S. Longhi, and A. Szameit, Topological triple phase transition in non-Hermitian Floquet quasicrystals, Nature (London) **601,** 354 (2022).

[19] S. Ganeshan, K. Sun, and S. Das Sarma, Topological Zero-Energy Modes in Gapless Commensurate Aubry-André-Harper Models, Phys. Rev. Lett. **110,** 180403 (2013).

[20] G. Semeghini, H. Levine, A. Keesling, S. Ebadi, T. T. Wang, D. Bluvstein, R. Verresen, H. Pichler, M. Kalinowski, R. Samajdar, A. Omran, S. Sachdev, A. Vishwanath, M. Greiner, V. Vuletić, and M. D. Lukin, Probing topological spin liquids on a programmable quantum simulator, Science **374,** 1242 (2021).

[21] K. J. Satzinger *et al.*, Realizing topologically ordered states on a quantum processor, Science **374,** 1237 (2021).

[22] X. Mi *et al.*, Noise-resilient edge modes on a chain of superconducting qubits, Science **378,** 785 (2022).

[23] J. Preskill, Quantum computing in the NISQ era and beyond, Quantum **2,** 79 (2018).

[24] I. M. Georgescu, S. Ashhab, and F. Nori, Quantum simulation, Rev. Mod. Phys. **86,** 153 (2014).

[25] A. J. Daley, I. Bloch, C. Kokail, S. Flannigan, N. Pearson, M. Troyer, and P. Zoller, Practical quantum advantage in quantum simulation, Nature (London) **607,** 667 (2022).

[26] C. Leefmans, A. Dutt, J. Williams, L. Yuan, M. Parto, F. Nori, S. Fan, and A. Marandi, Topological dissipation in a time-multiplexed photonic resonator network, Nat. Phys. **18,** 442 (2022).

[27] B. Cheng *et al.*, Noisy intermediate-scale quantum computers, Front. Phys. **18,** 21308 (2023).

[28] Z. Yan, Y. R. Zhang, M. Gong, Y. Wu, Y. Zheng, S. Li, C. Wang, F. Liang, J. Lin, Y. Xu, C. Guo, L. Sun, C. Z. Peng, K. Xia, H. Deng, H. Rong, J. Q. You, F. Nori, H. Fan, X. Zhu, and J. W. Pan, Strongly correlated quantum walks with a 12-qubit superconducting processor, Science **364,** 753 (2019).

[29] W. Cai, J. Han, F. Mei, Y. Xu, Y. Ma, X. Li, H. Wang, Y. P. Song, Z.-Y. Xue, Z.-q. Yin, S. Jia, and L. Sun, Observation of Topological Magnon Insulator States in a Superconducting Circuit, Phys. Rev. Lett. **123,** 080501 (2019).

[30] S. K. Zhao, Z.-Y. Ge, Z. Xiang, G. M. Xue, H. S. Yan, Z. T. Wang, Z. Wang, H. K. Xu, F. F. Su, Z. H. Yang, H. Zhang, Y.-R. Zhang, X.-Y. Guo, K. Xu, Y. Tian, H. F. Yu, D. N. Zheng, H. Fan, and S. P. Zhao, Probing Operator Spreading via Floquet Engineering in a Superconducting Circuit, Phys. Rev. Lett. **129,** 160602 (2022).

[31] S. Denisov, S. Flach, and P. Hänggi, Tunable transport with broken space-time symmetries, Phys. Rep. **538,** 77 (2014).

[32] Y. Wu, L.-P. Yang, M. Gong, Y. Zheng, H. Deng, Z. Yan, Y. Zhao, K. Huang, A. D. Castellano, W. J. Munro, K. Nemoto, D.-N. Zheng, C. P. Sun, Y.-x. Liu, X. Zhu, and L. Lu, An efficient and compact switch for quantum circuits, npj Quantum Inf. **4,** 50 (2018).

[33] M. Reagor *et al.*, Demonstration of universal parametric entangling gates on a multi-qubit lattice, Sci. Adv. **4,** eaao360 (2018).

[34] H. Lignier, C. Sias, D. Ciampini, Y. Singh, A. Zenesini, O. Morsch, and E. Arimondo, Dynamical Control of Matter-Wave Tunneling in Periodic Potentials, Phys. Rev. Lett. **99,** 220403 (2007).

[35] A. Eckardt, Colloquium: Atomic quantum gases in periodically driven optical lattices, Rev. Mod. Phys. **89,** 011004 (2017).

[36] See Supplemental Material at http://link.aps.org/supplemental/10.1103/PhysRevLett.131.080401 which includes Refs. [37–39] for the information on sample fabrication, experimental methods, and additional discussion.

[37] Z. Chen, A. Megrant, J. Kelly, R. Barends, J. Bochmann, Y. Chen, B. Chiaro, A. Dunsworth, E. Jeffrey, J. Y. Mutus, P. J. O'Malley, C. Neill, P. Roushan, D. Sank, A. Vainsencher, J. Wenner, T. C. White, A. N. Cleland, and J. M. Martinis, Fabrication and characterization of aluminum airbridges for superconducting microwave circuits, Appl. Phys. Lett. **104,** 052602 (2014).

[38] J. Koch, T. M. Yu, J. Gambetta, A. A. Houck, D. I. Schuster, J. Majer, A. Blais, M. H. Devoret, S. M. Girvin, and R. J. Schoelkopf, Charge-insensitive qubit design derived from the Cooper pair box, Phys. Rev. A **76,** 042319 (2007).

[39] S. Ryu and Y. Hatsugai, Topological Origin of Zero-Energy Edge States in Particle-Hole Symmetric Systems, Phys. Rev. Lett. **89,** 077002 (2002).

[40] I. I. Satija and G. G. Naumis, Chern and Majorana modes of quasiperiodic systems, Phys. Rev. B **88,** 054204 (2013).

[41] W. DeGottardi, D. Sen, and S. Vishveshwara, Majorana Fermions in Superconducting 1D Systems Having Periodic, Quasiperiodic, and Disordered Potentials, Phys. Rev. Lett. **110,** 146404 (2013).

[42] D. J. Thouless, M. Kohmoto, M. P. Nightingale, and M. den Nijs, Quantized Hall Conductance in a Two-Dimensional Periodic Potential, Phys. Rev. Lett. **49,** 405 (1982).

[43] A. Bansil, H. Lin, and T. Das, Colloquium: Topological band theory, Rev. Mod. Phys. **88,** 021004 (2016).

[44] W. P. Su, J. R. Schrieffer, and A. J. Heeger, Solitons in Polyacetylene, Phys. Rev. Lett. **42,** 1698 (1979).

[45] C. Schweizer, F. Grusdt, M. Berngruber, L. Barbiero, E. Demler, N. Goldman, I. Bloch, and M. Aidelsburger, Floquet approach to $\mathbb{Z}_2$ lattice gauge theories with ultracold atoms in optical lattices, Nat. Phys. **15,** 1168 (2019).

[46] Y. Wu, W. Liu, J. Geng, X. Song, X. Ye, C.-K. Duan, X. Rong, and J. Du, Observation of parity-time symmetry breaking in a single-spin system, Science **364,** 878 (2019).